K-Doping Dependence of the Fermi Surface of the Iron-Arsenic $Ba_{1-x}K_xFe_2As_2$ Superconductor Using Angle-Resolved Photoemission Spectroscopy

Chang Liu,[1] G. D. Samolyuk,[1] Y. Lee,[1] Ni Ni,[1] Takeshi Kondo,[1] A. F. Santander-Syro,[2,3] S. L. Bud'ko,[1] J. L. McChesney,[4] E. Rotenberg,[4] T. Valla,[5] A. V. Fedorov,[4] P. C. Canfield,[1] B. N. Harmon,[1] and A. Kaminski[1]

[1]*Ames Laboratory and Department of Physics and Astronomy, Iowa State University, Ames, Iowa 50011, USA*
[2]*Laboratoire Photons Et Matière, UPR-5 CNRS, ESPCI, 10 rue Vauquelin, 75231 Paris cedex 5, France*
[3]*Labratoire de Physique des Solides, UMR-8502 CNRS, Université Paris-Sud, Bât. 510, 91405 Orsay, France*
[4]*Advanced Light Source, Berkeley National Laboratory, Berkeley, California 94720, USA*
[5]*Condensed Matter Physics and Materials Science Department, Brookhaven National Laboratory, Upton, New York 11973, USA*

(Received 20 June 2008; published 24 October 2008)

We use angle-resolved photoemission spectroscopy to investigate the electronic properties of the newly discovered iron-arsenic superconductor $Ba_{1-x}K_xFe_2As_2$ and nonsuperconducting $BaFe_2As_2$. Our study indicates that the Fermi surface of the undoped, parent compound $BaFe_2As_2$ consists of hole pocket(s) at Γ (0,0) and larger electron pocket(s) at X (1,0), in general agreement with full-potential linearized plane wave calculations. Upon doping with potassium, the hole pocket expands and the electron pocket becomes smaller with its bottom approaching the chemical potential. Such an evolution of the Fermi surface is consistent with hole doping within a rigid-band shift model. Our results also indicate that the full-potential linearized plane wave calculation is a reasonable approach for modeling the electronic properties of both undoped and K-doped iron arsenites.

DOI: 10.1103/PhysRevLett.101.177005 PACS numbers: 74.25.Jb, 74.62.Dh, 74.70.−b, 79.60.−i

Iron-arsenic based materials comprise a very interesting class of materials with many unusual properties. For example, they have recently been shown to be superconducting with a T_c as high as 55 K [1–3]. This discovery has initiated a frenzy of research activity, which until very recently was limited to studies of only polycrystalline samples. Initial experiments focused on fluorine-doped rare earth oxide based materials (RFeAsOF) [4–6]. To date, there is very little photoemission data available on these compounds [7–9] with only one angle-resolved study [10]. The recent discovery of superconductivity in oxygen-free $Ba_{1-x}K_xFe_2As_2$ [11] suggests that the superconductivity is ultimately linked to the electronic properties of the iron-arsenic layer(s) with the remaining layers acting as a charge reservoir. This scheme closely resembles the situation found in the cuprates. In both $BaFe_2As_2$ and $SrFe_2As_2$ there are clear structural phase transitions from a high temperature tetragonal to low temperature orthorhombic phases [12–14]. When potassium is substituted for barium, the temperature at which the structural transition occurs is suppressed and superconductivity emerges [11,13]. Some experiments also point to the existence of a transition into a spin density wave (SDW) state at higher temperature [5,15] and related changes of the electronic structure [16]. The mechanism of pairing in these new high temperature superconductors is not known. It is quite possible that this is a new path to establishing superconductivity, different from both the classical electron-phonon interaction and from the one that occurs in cuprates. The emergence of superconductivity [11,13] in iron-arsenic system upon the suppression of structural and SDW transitions [5,15] hints at a possible magnetic origin of pairing [17,18]. The topology of the Fermi surface is considered crucially important for both establishing the SDW order and superconductivity in these materials since the former does and the latter may depend on nesting conditions. Determining the effects of doping on low lying electronic excitations is therefore essential for understanding these materials. It is equally important to understand the electronic properties of the parent compound because undoped systems are easier to model theoretically, and they represent a basis for higher order approximations. The information about its electronic structure and evolution with doping is deemed essential to formulate a successful model of superconductivity in these fascinating systems.

The recent growth of large, high quality single crystals [13] has opened up the possibility of examining the electronic properties of these materials. Here we present angle-resolved photoemission spectroscopy (ARPES) data on the Fermi surface and band dispersion of $Ba_{1-x}K_xFe_2As_2$, and discuss how they are affected by doping with potassium. We find in the undoped samples, the Fermi surface consists of a smaller hole pocket(s) centered at Γ (0,0,0) and a larger electron pocket(s) located at each of the X points. Upon doping with potassium, the Γ hole pocket increases in size and the X pocket contracts. There are also significant shifts in energy for lower lying, fully occupied bands. In the potassium-doped system the bottom of the X band is located in close proximity to the chemical potential. This is significant for the emergence of the superconductivity upon doping. Our experimental results are in general

agreement with band calculations for both undoped and doped system.

Single crystals of the parent compound, $BaFe_2As_2$, and potassium-doped samples, $Ba_{1-x}K_xFe_2As_2$, with an approximate doping $x = 0.45$ were grown out of a Sn flux using conventional high temperature solution growth techniques [13]. Large (up to 2×2 mm) single crystals were cleaved *in situ* yielding flat mirrorlike surfaces. The experimental data were acquired using a laboratory-based ARPES system consisting of a Scienta SES2002 electron analyzer, GammaData UV lamp and custom designed refocusing optics at Iowa State University. The samples were cooled using a closed-cycle refrigerator. Measurements were performed on several samples; they all yielded similar results for the band dispersion and Fermi surface. All data were acquired using the HeII line with a photon energy of 40.8 eV. The momentum resolution was set at 0.014 $Å^{-1}$ and 0.06 $Å^{-1}$ parallel and perpendicular to the slit direction. The energy resolution was 30 meV for the Fermi surface scans and 15 meV for the intensity maps. All measurements are taken at $T = 100$ K. Our full-potential linearized plane wave (FLAPW) calculations [19] used the local density approximation [20], and the experimental lattice constants [11] for the undoped parent compound $BaFe_2As_2$ and potassium-doped $Ba_{1-x}K_xFe_2As_2$ with $x = 0.4$. Total energy minimization was used to determine the z location of the arsenic atom $z_{As} = 0.341c$.

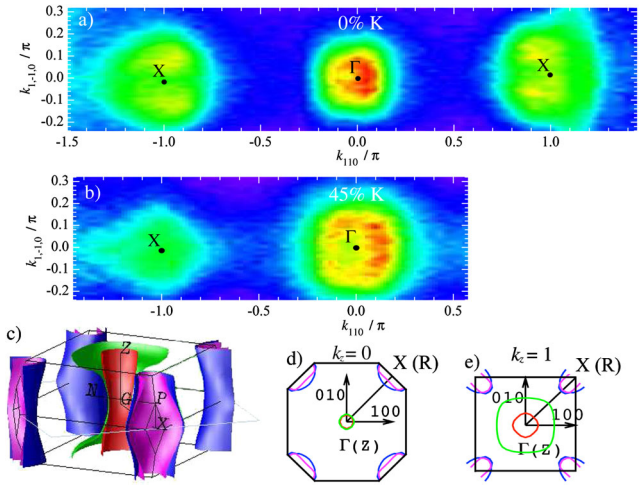

FIG. 1 (color online). Measured Fermi surface (FS) of $BaFe_2As_2$ and $Ba_{1-x}K_xFe_2As_2$ and calculated FS for undoped case. (a) FS map of $BaFe_2As_2$—intensity of the photoelectrons integrated over 20 meV about the chemical potential obtained with 40.8 eV photons. Experiment was done at $T = 100$ K. Areas of bright color mark the locations of the FS. (b) FS map of $Ba_{1-x}K_xFe_2As_2$ with nominal $x = 0.45$ measured under the same conditions as (a). (c) 3-dimensional FS of $BaFe_2As_2$ obtained from FLAPW calculations. (d) FS cross section for $k_z = 0$ (X-Γ plane) obtained by FLAPW calculations. (e) Same as (d) but for $k_z = 1$ (R-Z plane).

The shape of the Fermi surface (FS) is normally illustrated by plotting the photoelectron intensity at the chemical potential [21,22]. In Figs. 1(a) and 1(b) we plot this quantity integrated within 20 meV of the chemical potential for the undoped and potassium-doped samples. The Fermi surface of undoped $BaFe_2As_2$ consists of a smaller circular-shaped hole pocket centered at Γ and larger electron pockets at X points with a characteristic "starrish" shape [more clearly seen in Fig. 2(a)], in reasonable agreement with the FLAPW calculations shown in Figs. 1(c)–1(e). In the potassium-doped samples [Fig. 1(b)] one can see that the Γ pocket becomes larger and the X pocket decrease in size, as compared to the undoped samples. This observation is consistent with hole doping of the material. Although there is also a variation in the intensity around the Γ and X pockets, it is only a signature of photoemission matrix elements and not the material itself.

In Fig. 2 we show how the shapes of both the Γ and X bands evolve with binding energy as well as potassium doping. With increasing binding energy, the contour of the Γ pocket becomes larger—consistent with its holelike topology, while the X pocket becomes smaller—consistent with its electronlike topology. One notable fact shown in Fig. 2 is that the size of the pockets at a binding energy 0.04 eV in the parent compound are similar to those of the potassium-doped compound at the Fermi level. In other words, based on a rigid-band shifting scenario, we could approximately say that the potassium hole doping lowers the chemical potential by ~40 meV. We note also that with potassium doping the bottom of the X band is located in very close proximity to the chemical potential.

In Fig. 3 we plot the experimental band dispersion data perpendicular to the Γ-X direction along cuts through the X and Γ points (i.e., along the $k_{1,-1,0}$ direction). For both the $x = 0$ and $x = 0.45$ doping levels, the hole pockets at Γ and the electron pockets at X are shown (see also Fig. 2) and are in general agreement with band calculations. Here we can examine the relative size of the hole pockets and the electron pockets in more detail by studying the Fermi crossing momenta (k_Fs) marked by darker curves in Figs. 3(c), 3(d), 3(h), and 3(i). These k_Fs were determined from the most intense points in the momentum distribution curves at the Fermi level. The number of k curves between two k_Fs is proportional to the actual size of each pocket.

The calculated Fermi surface [Fig. 3(e)] of $BaFe_2As_2$ is quite similar to the well-studied LaFeAsO [23,24]. Like LaFeAsO, a detailed calculation of $BaFe_2As_2$ is sensitive to the z location of As [25]. When z_{As} is changed from the experimental value to the one determined by energy minima calculations, we found that the Γ hole pocket [shown in the middle of Fig. 1(c)] changes from a cylinder without dispersion along the k_z direction [24] to a modulated cylinder with strong dispersion along k_z. The band structure for the doped material performed using the virtual

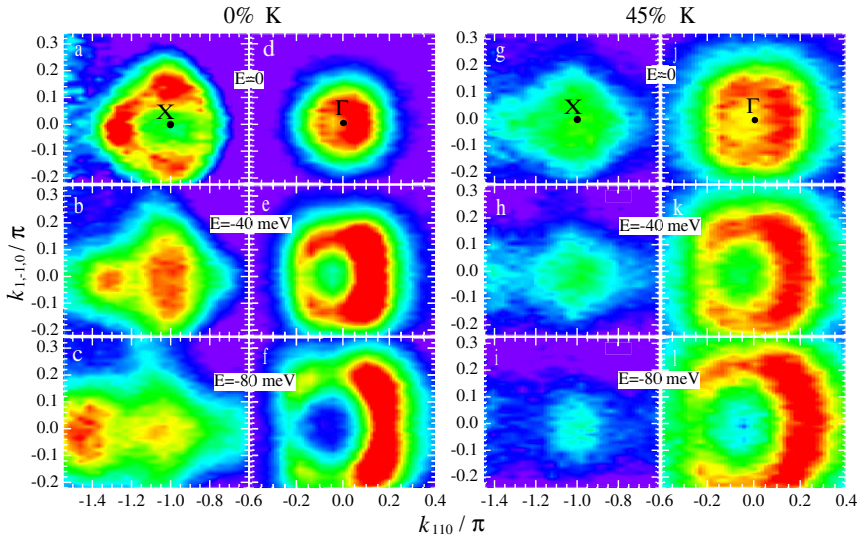

FIG. 2 (color online). Electron intensity map for selected binding energies of the undoped and potassium-doped samples. All data were taken at $T = 100$ K. Panels (a)–(f) present the data of undoped $BaFe_2As_2$, while panels (g)–(l) present the data of $Ba_{1-x}K_xFe_2As_2$ with nominal $x = 0.45$. The three rows of panels present the data at the chemical potential E_F, binding energy $E = 0.04$, and 0.08 eV, respectively; the two columns of panels for each doping present the intensity map covering a k-space area near the X point [(a)–(c), (g)–(i)] and the Γ point [(d)–(f), (j)–(l)], respectively.

crystal method is shown in Fig. 3(j). Clearly, in the undoped parent compound, both experiment and calculation give the X pocket as larger than the Γ pocket, whereas in the $x = 0.45$ potassium-doped samples, the opposite is the case. This effect is consistent with the idea of rigid-band shifting, namely, potassium doping lowers the chemical potential of the parent compound, while the shapes of the bands are left unchanged. A second notable doping dependent feature is the energy shift of two fully occupied bands, marked by black arrows in Figs. 3(b), 3(e), 3(g), and 3(j),

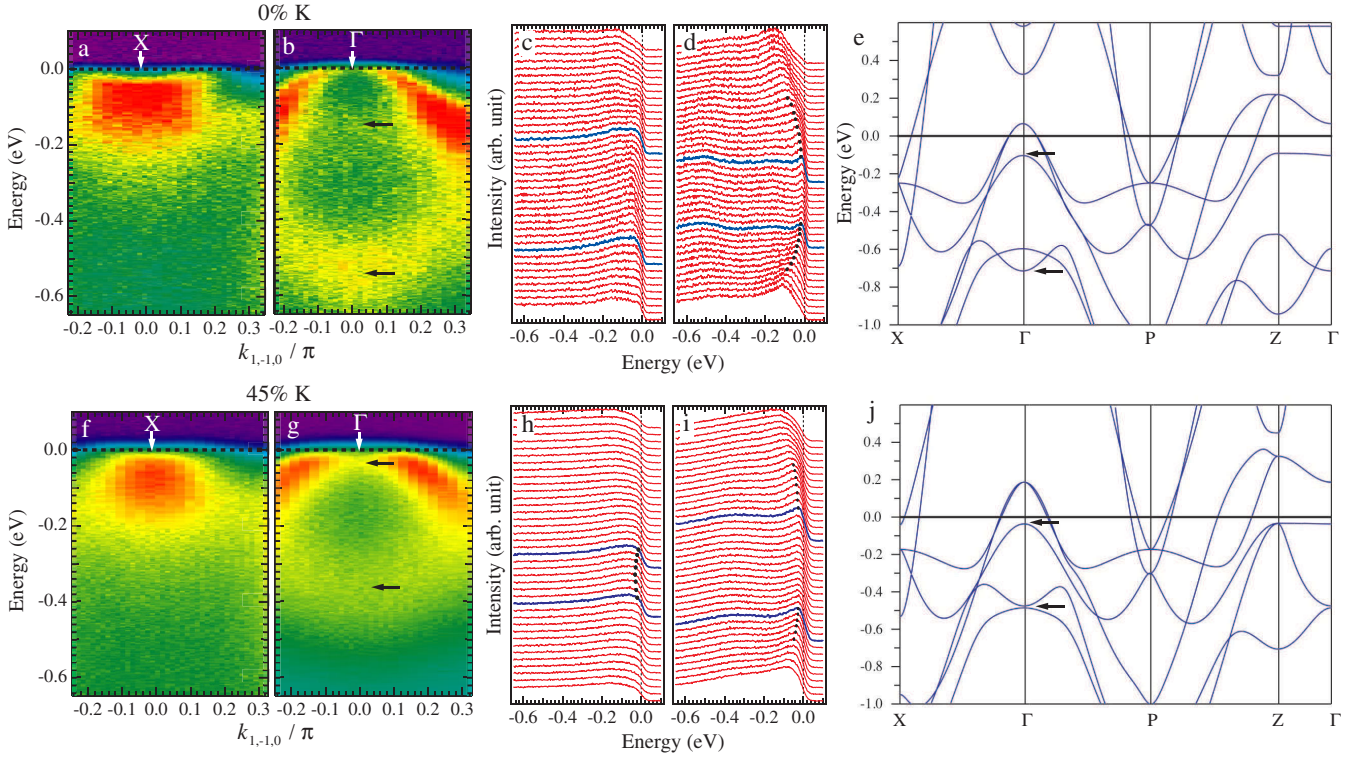

FIG. 3 (color online). Experimental band dispersions and corresponding energy distribution curves (EDCs) along selected cuts, compared with theoretical band structure. Panels (a)–(e) present the data of undoped $BaFe_2As_2$, while panels (f)–(j) present the data of $Ba_{1-x}K_xFe_2As_2$ with nominal $x = 0.45$. (a) ARPES intensity map in the X region for undoped sample. (b) ARPES intensity map in the Γ region for undoped sample. (c, d) EDCs for the same cuts in (a) and (b). Curves at Fermi momenta are darker. (e) Results of FLAPW band calculation for parent compound $BaFe_2As_2$. (f) ARPES intensity map in X region for doped sample $x = 0.45$. (g) ARPES intensity map in Γ region for doped sample $x = 0.45$. (h, i) EDCs for the same cuts in (f) and (g). Curves at Fermi momenta are darker. (j) Results of FLAPW band calculation for doped $Ba_{1-x}K_xFe_2As_2$ with $x = 0.45$.

where Fig. 3(e) and 3(j) plot the calculated band structure of the undoped $BaFe_2As_2$ and potassium-doped $Ba_{1-x}K_xFe_2As_2$ with $x = 0.45$, respectively. These arrows point to similar characteristic features in experimental data and calculations and how they change upon doping. On potassium doping, the upper band shifts to lower binding energy by ~130 meV, while the lower band shifts to lower binding energy by ~180 meV. This fact is in qualitative agreement with the calculations. A third feature notable in Fig. 3 is the missing of bilayer splitting in the measured data. This fact also agrees well with the FLAPW calculations, where the two bands constructing the Fermi surface are highly degenerated in both the undoped and *K*-doped systems. All these doping dependent features point to the conclusion that the FLAPW approximation is valid in both undoped and hole-doped iron-arsenic superconductors.

Despite the fact that our potassium-doped samples display bulk superconductivity, we did not detect a superconducting gap in the ARPES measurement down to 12 K. This may be due to a loss of potassium from the surface in the ultrahigh vacuum environment or possibly a variation in potassium doping between different layers, which suggests a strong dependence of the critical temperature upon doping. Our data also indicate that upon further doping to a point where the material becomes superconducting, the bottom of the *X* pocket will be in very close proximity to the chemical potential. Such an increase of the density of states (DOS) may be relevant to the emergence of superconductivity in these materials.

In conclusion we have determined the evolution of the Fermi surface and band dispersion for $Ba_{1-x}K_xFe_2As_2$ for $x = 0$ and $x = 0.45$. We find that in the undoped samples, the Fermi surface consists of a smaller hole pocket(s) centered at Γ (0,0,0) and a larger electron pocket(s) located at each of the *X* points. This is in general agreement with band calculations. Upon doping, the Γ hole pocket increases in size and the *X* pocket contracts, which is consistent with hole doping. The conduction bands shift in energy in a similar fashion, in accordance with a rigid-band shift scheme. Our results are consistent with the scenario that doping leads to a suppression of SDW order [18], because we observe opposite changes in the size of the Γ and *X* pockets, which worsens the nesting conditions with increasing potassium concentration. Our data also indicates that upon further doping to a point where the material becomes superconducting, the bottom of the *X* pocket will be in very close proximity to the chemical potential. The consequent increase in the DOS may be relevant for the emergence of superconductivity in these materials.

We are grateful for useful discussions with Jörg Schmalian. We thank Helen Fretwell for useful remarks and corrections. Work at Ames Laboratory was supported by the Department of Energy Basic Energy Sciences under Contract No. DE-AC02-07CH11358. ALS is operated by the US DOE under Contract No. DE-AC03-76SF00098. Brookhaven National Laboratory is supported by US DOE under Contract No. DE-AC02-98CH10886. A. F. S. S. thanks LPEM for financial support.

[1] Yoichi Kamihara, Takumi Watanabe, Masahiro Hirano, and Hideo Hosono, J. Am. Chem. Soc. **130**, 3296 (2008).
[2] Hiroki Takahashi *et al.*, Nature (London) **453**, 376 (2008).
[3] Ren Zhi-An *et al.*, Chin. Phys. Lett. **25**, 2215 (2008).
[4] T. Y. Chen, Z. Tesanovic, R. H. Liu, X. H. Chen, and C. L. Chien, Nature (London) **453**, 1224 (2008).
[5] Clarina de la Cruz *et al.*, Nature (London) **453**, 899 (2008).
[6] F. Hunte *et al.*, Nature (London) **453**, 903 (2008).
[7] T. Sato *et al.*, J. Phys. Soc. Jpn. (to be published).
[8] Xiaowen Jia *et al.*, Chin. Phys. Lett. **25**, 3765 (2008).
[9] Haiyun Liu *et al.*, Chin. Phys. Lett. **25**, 3761 (2008).
[10] C. Liu *et al.*, arXiv:0806.2147.
[11] M. Rotter, M. Tegel, and D. Johrendt, Phys. Rev. Lett. **101**, 107006 (2008).
[12] M. Rotter *et al.*, Phys. Rev. B **78**, 020503(R) (2008).
[13] N. Ni *et al.*, Phys. Rev. B **78**, 014507 (2008).
[14] J.-Q. Yan *et al.*, Phys. Rev. B **78**, 024516 (2008).
[15] X. F. Wang *et al.*, arXiv:0806.2452.
[16] L. X. Yang *et al.*, arXiv:0806.2627.
[17] I. I. Mazin, D. J. Singh, M. D. Johannes, and M. H. Du, Phys. Rev. Lett. **101**, 057003 (2008).
[18] V. Cvetkovic and Z. Tesanovic, arXiv:0804.4678v3.
[19] P. Blaha, K. Schwarz, G. K. Madsen, D. Kvasnick, and J. Luitz, *WIEN2K, An Augmented Plane Wave + Local Orbitals Program for Calculation Crystal Properties* (K. Schwarz, TU Wien, Austria, 2001), ISBN 3-9501031-1-2.
[20] J. P. Perdew and Y. Wang, Phys. Rev. B **45**, 13244 (1992).
[21] J. Mesot *et al.*, Phys. Rev. B **63**, 224516 (2001).
[22] H. M. Fretwell *et al.*, Phys. Rev. Lett. **84**, 4449 (2000).
[23] D. J. Singh and M.-H. Du, Phys. Rev. Lett. **100**, 237003 (2008).
[24] I. A. Nekrasov, Z. V. Pchelkina, and M. V. Sadovskii, JETP Lett. **87**, 560 (2008).
[25] I. I. Mazin, M. D. Johannes, L. Boeri, K. Koepernik, and D. J. Singh, Phys. Rev. B **78**, 085104 (2008).